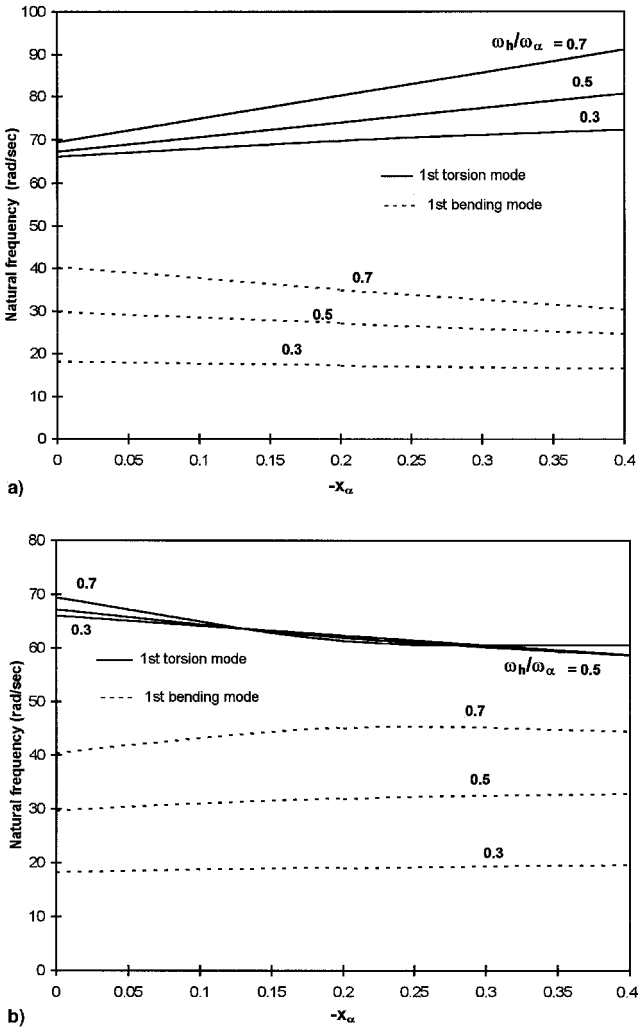

Fig. 3 Natural frequencies for the first bending and torsional modes against x_α for selected values of frequency ratio ω_h/ω_α for ψ = a) 0.4 and b) −0.4.

and ω_α are uncoupled fundamental bending and torsional natural frequencies that are both independent of x_α and ψ, whereas the plotted graphs shown by solid and dashed lines represent fundamental bending and torsional coupled natural frequencies, respectively. It is clear from Fig. 3a that as the negative x_α increases, the frequency difference between the two vibrational modes of interest increases and as a consequence flutter speed also increases, thus reinforcing the importance of modal coupling in such studies.[10]

In contrast, when negative ψ ($\psi = -0.4$ in this case) is present together with negative x_α (see Fig. 3b), frequency convergence occurs between the two modes of interest, and as a result the flutter speed reduces. The preceding frequency phenomenon was also noticed by Weisshaar and Foist,[7] but not from an aeroelastic point of view, so that its effect on flutter behavior was not reported.

From the preceding results, it can be concluded that the wash-out behavior of a composite wing can be useful in increasing its flutter speed when the mass axis is well behind the shear center of the wing cross section as opposed to the corresponding case when the wing exhibits wash-in behavior. The investigation has also revealed that for certain combinations of positive ψ and negative x_α, the flutter speed is unaffected by changes in the frequency ratio ω_h/ω_α.

References

[1]Austin, F., Hadcock, R., Hutchings, D., Sharp, D., Tang, S., and Waters, C., "Aeroelastic Tailoring of Advanced Composite Lifting Surfaces," *Proceedings of the AIAA/ASME/SAE 17th Structures, Structural Dynamics, and Materials Conference*, AIAA, New York, 1976, pp. 69–79.

[2]Shirk, M. H., Hertz, T. J., and Weisshaar, T. A., "Aeroelastic Tailoring—Theory, Practice, and Promise," *Journal of Aircraft*, Vol. 23, No. 1, 1986, pp. 6–18.

[3]Weisshaar, T. A., and Ryan, R. J., "Control of Aeroelastic Instabilities Through Stiffness Cross-Coupling," *Journal of Aircraft*, Vol. 23, No. 2, 1986, pp. 148–155.

[4]Lottati, I., "Flutter and Divergence Aeroelastic Characteristics for Composite Forward Swept Cantilevered Wing," *Journal of Aircraft*, Vol. 22, No. 11, 1985, pp. 1001–1007.

[5]Georghiades, G. A., Guo, S., and Banerjee, J. R., "Flutter Characteristics of Laminated Composite Wings," *Journal of Aircraft*, Vol. 33, No. 6, 1996, pp. 1204–1206.

[6]Georghiades, G. A., and Banerjee, J. R., "Flutter Prediction for Composite Wings Using Parametric Studies," *AIAA Journal*, Vol. 35, No. 4, 1997, pp. 746–748.

[7]Weisshaar, T. A., and Foist, B. L., "Vibration Tailoring of Advanced Composite Lifting Surfaces," *Journal of Aircraft*, Vol. 22, No. 2, 1985, pp. 141–147.

[8]Banerjee, J. R., and Williams, F. W., "Free Vibration of Composite Beams—An Exact Method Using Symbolic Computation," *Journal of Aircraft*, Vol. 32, No. 3, 1995, pp. 636–642.

[9]Banerjee, J. R., "Use and Capability of CALFUN—A Program for Calculation of Flutter Speed Using Normal Modes," *Proceedings of the International AMSE Conference on Modelling & Simulation* (Athens, Greece), Vol. 3.1, AMSE Press, Tassin-la-Demi-Lune, France, 1984, pp. 121–131.

[10]Georghiades, G. A., and Banerjee, J. R., "Role of Modal Interchange on the Flutter of Laminated Composite Wings," *Journal of Aircraft*, Vol. 35, No. 1, 1998, pp. 157–161.

Perturbation Solution of Dynamic Stability Derivatives over Pointed Bodies of Revolution

Guowei Yang* and Etsuo Morishita†
University of Tokyo, Tokyo 113, Japan

Introduction

THE unsteady Euler and Navier–Stokes equations represent adequate mathematical models for unsteady transonic flow. Time-accurate solutions of the Euler and Navier–Stokes equations are computationally expensive, particularly in the low-frequency range. But the linearized theory fails in calculating transonic flows. For engineering applications, a compromise perturbation theory that considers the nonlinear effects for transonic flow and also avoids massive time-accurate computation for low reduced frequencies is developed in this paper.

The theory is simplified by introducing a perturbation approach. The unsteady flow is decomposed into a mean steady motion and unsteady perturbation components. The mean steady flow is then described by a nonlinear equation, and the unsteady perturbed flow is described by a complex linear equation, with variable coefficients determined by the mean steady flow.

Here, for simplicity, the sharp-nosed body of revolution undergoing pitching oscillations around zero incidence is considered. Because the flow past a body of revolution at zero in-

Received Nov. 16, 1997; revision received April 27, 1998; accepted for publication May 7, 1998.

*Visiting Scholar, on leave from University of Science and Technology of China, Hefei, Anhui 230026, PRC.

†Professor. Department of Aeronautics and Astronautics.

cidence is a two-dimensional axisymmetric flow, this avoids having to solve a three-dimensional equation. For a sharp-nosed body, the flow is not separated on the leeward side, even at moderate incidence. Thus, the inviscid theory becomes valid and a cosine variation of quantities in the crossflow plane may be assumed. In this approximation, the control equations and their boundary conditions have been deduced, and the pressure coefficient and dynamic stability derivatives for pointed bodies of revolution are calculated.

Formulation

The conservation form of the unsteady Euler equations in a body-axes frame is given by

$$\frac{\partial \boldsymbol{Q}}{\partial t} + \frac{\partial \boldsymbol{E}}{\partial \xi} + \frac{\partial \boldsymbol{F}}{\partial \eta} + \frac{\partial \boldsymbol{G}}{\partial \zeta} = H \tag{1}$$

Here, t is the time and (ξ, η, ζ) is the body-conformed curvilinear coordinate system; In Eq. (1), $\boldsymbol{Q}$ is the vector of dependent flow variables; $\boldsymbol{E}$, $\boldsymbol{F}$, and $\boldsymbol{G}$ are the inviscid vectors; and H is source item.

For flows about a body of revolution undergoing a small-amplitude harmonic oscillation at zero incidence (except the circumferential velocity component), a cosine variation of the flow quantities in the circumferential direction can be assumed. Using R represents any one of the flow quantities, ρ, u, v, p, or e, and it can be decomposed into a mean steady and an unsteady component:

$$R(\xi, \eta, \varsigma, t) = R_0(\xi, \eta) + \alpha_0 R_1 \cos \varsigma e^{\omega t} + o(\alpha_0^2) \tag{2a}$$

For circumferential velocity component w, we assume

$$w(\xi, \eta, \varsigma, t) = \alpha_0 w_1 \sin \varsigma e^{\omega t} + o(\alpha_0^2) \tag{2b}$$

where the subscripts 0 and 1 refer to the mean and unsteady complex components, respectively; ω is the frequency of oscillation; and α_0 is the amplitude of oscillation motion.

By substituting Eqs. (2a) and (2b) into Eq. (1) and collecting terms of the zeroth order, one obtains the zeroth-order equations for the mean steady quantities

$$\frac{\partial E_0}{\partial \xi} + \frac{\partial F_0}{\partial \eta} = H_0 \tag{3}$$

$$E_0 = J^{-1}[\rho_0 U_0,\ \rho_0 u_0 U_0 + \xi_z p_0,\ \rho_0 v_0 U_0 + \xi_r p_0,\ (e_0 + p_0)U_0]^T$$

$$F_0 = J^{-1}[\rho_0 V_0,\ \rho_0 u_0 V_0 + \eta_z p_0,\ \rho_0 v_0 V_0 + \eta_r p_0,\ (e_0 + p_0)V_0]^T$$

$$H_0 = -(Jr)^{-1}[\rho_0 v_0,\ \rho_0 u_0 v_0,\ \rho_0 v_0^2,\ (e_0 + p_0)v_0]^T$$

$$U_0 = \xi_z u_0 + \xi_r v_0, \qquad V_0 = \eta_z u_0 + \eta_r v_0$$

The first-order equations for real and imaginary parts of the unsteady component are

$$\frac{\partial E_{1r}}{\partial \xi} + \frac{\partial F_{1r}}{\partial \eta} = H_{1r} + \omega Q_{1i} + G_{1r} \tag{4a}$$

$$\frac{\partial E_{1i}}{\partial \xi} + \frac{\partial F_{1i}}{\partial \eta} = H_{1i} - \omega Q_{1r} + G_{1i} \tag{4b}$$

here, the unified expressions of the real and imaginary parts are given

$$E_{1j} = J^{-1}[\rho_0 U_{1j} + \rho_{1j} U_0,\ (\rho_{1j} u_0 + \rho_0 u_{1j})U_0 + \rho_0 u_0 U_{1j} + \xi_z p_{1j}$$
$$(\rho_{1j} v_0 + \rho_0 v_{1j})U_0 + \rho_0 v_0 U_{1j} + \xi_r p_{1j},\ \rho_0 U_0 w_{1j},\ (e_0 + p_0)U_{1j}$$
$$+ (e_{1j} + p_{1j})U_0]^T$$

$$F_{1j} = J^{-1}[\rho_0 V_{1j} + \rho_{1j} V_0,\ (\rho_{1j} u_0 + \rho_0 u_{1j})V_0 + \rho_0 u_0 V_{1j} + \eta_z p_{1j}$$
$$(\rho_{1j} v_0 + \rho_0 v_{1j})V_0 + \rho_0 v_0 V_{1j} + \eta_r p_{1j},\ \rho_0 V_0 w_{1j},\ (e_0 + p_0)V_{1j}$$
$$+ (e_{1j} + p_{1j})V_0]^T$$

$$H_{1j} = -(Jr)^{-1}[\rho_0 v_{1j} + \rho_{1j} v_0,\ \rho_0 u_0 v_{1j} + \rho_0 v_0 u_{1j} + \rho_{1j} u_0 v_0$$
$$2\rho_0 v_0 v_{1j} + \rho_{1j} v_0^2,\ 2\rho_0 v_0 w_{1j},\ (e_0 + p_0)v_{1j} + v_0(e_{1j} + p_{1j})]^T$$

$$G_{1j} = -(Jr)^{-1}[\rho_0 w_{1j},\ \rho_0 u_0 w_{1j},\ \rho_0 v_0 w_{1j},\ -p_{1j},\ (e_0 + p_0)w_{1j}]^T$$

$$U_{1j} = \xi_z u_{1j} + \xi_r v_{1j},\ V_{1j} = \eta_z u_{1j} + \eta_r v_{1j}$$

$$e_{1j} = \rho_0(u_0 u_{1j} + v_0 v_{1j}) + 0.5 p_{1j}(u_0^2 + v_0^2) + p_{1j}/(\gamma - 1)$$

where the subscript j is taken as r, i, which refer to the real and imaginary parts of unsteady components.

The first-order equation is a linearized equation, its Jacobian coefficient matrix being determined by the zeroth-order equations. The numerical calculation of the unsteady motion is reduced to solving three coupled "steady" equations.

Boundary Conditions

For the oscillating body, the surface boundary condition $\boldsymbol{V}\cdot\boldsymbol{n} = U_n$ is imposed. By substituting Eq. (2) into the condition and collecting terms of the same order, the zeroth-order and first-order surface boundary conditions can be obtained:

$$-u_0 \sin\delta + v_0 \cos\delta = 0 \quad \text{(zeroth-order)} \tag{5a}$$

$$\begin{aligned} &-u_{1r} \sin\delta + v_{1r} \cos\delta = 0 \\ &-u_{1i} \sin\delta + v_{1i} \cos\delta = -\omega[z \cos\delta + f(z)\sin\delta] \end{aligned} \quad \text{(first-order)} \tag{5b}$$

here $\boldsymbol{V}$ is the velocity of the fluid, $\boldsymbol{n}$ is the unit normal to the moving surface, δ is the inclination angles of body surface in the meridian plane, and U_n is the velocity component of the moving surface in the normal direction.

In the far field, we use nonreflecting boundary conditions based on the local Riemann unvariables. At the downstream boundary, a simple zero-axial-gradient extrapolation condition was applied.

Obviously, the zeroth-order equations and boundary conditions are the same as axisymmetric steady equations and corresponding boundary conditions.

Pressure Coefficient and Dynamic Stability Derivatives

The surface pressure coefficient can be expressed by the perturbation approach as

$$C_p = C_{p0} + C_{\mathrm{pr}} \cos \varsigma\alpha(t) + \omega^{-1} C_{\mathrm{pi}} \cos \varsigma\dot{\alpha}(t) \tag{6}$$

At zero incidence, the pressure of the mean steady flow does not contribute to the pitching moment and dynamic stability derivative; hence they can be obtained only related to the first order quantities

$$C_m = \alpha R^{-3} \int_0^l C_{\mathrm{pr}}(z - z_c) f(z)\, \mathrm{d}z + \dot{\alpha}\omega^{-1} R^{-3} \int_0^l C_{\mathrm{pi}}(z - z_c) f(z)\, \mathrm{d}z \tag{7a}$$

so

$$C_{m\dot{\alpha}} + C_{mq} = \omega^{-1} R^{-3} \int_0^l C_{\mathrm{pi}}(z - z_c) f(z)\, \mathrm{d}z \tag{7b}$$

Because C_{pi} contains the effects of angle of attack and rotation, the derivative C_{mi} in Eq. (7a) should be written as $C_{mi} + C_{mq}$ in Eq. (7b). The reference area and length are assumed to be the base area and radius, with l being the length of the body of revolution.

Computation Method

Introducing time-correlating terms in Eqs. (3) and (4), the equations are revised into

$$\frac{\partial Q_0}{\partial t} + \frac{\partial E_0}{\partial \xi} + \frac{\partial F_0}{\partial \eta} = H_0 \tag{8a}$$

$$\frac{\partial Q_{1r}}{\partial t} + \frac{\partial E_{1r}}{\partial \xi} + \frac{\partial F_{1r}}{\partial \eta} = H_{1r} + \omega Q_{1i} + G_{1r} \tag{8b}$$

$$\frac{\partial Q_{1i}}{\partial rt} + \frac{\partial E_{1i}}{\partial \xi} + \frac{\partial F_{1i}}{\partial \eta} = H_{1i} - \omega Q_{1r} + G_{1i} \tag{8c}$$

$$Q_0 = J^{-1}[\rho_0,\ \rho_0 u_0,\ \rho_0 v_0,\ e_0]^T$$

$$Q_{1r} = J^{-1}[\rho_{1r},\ \rho_0 u_{1r} + \rho_{1r} u_0,\ \rho_0 v_{1r} + \rho_{1r} v_0,\ \rho_0 w_{1r},\ e_{1r}]^T$$

$$Q_{1i} = J^{-1}[\rho_{1i},\ \rho_0 u_{1i} + \rho_{1i} u_0,\ \rho_0 v_{1i} + \rho_{1i} v_0,\ \rho_0 w_{1i},\ e_{1i}]^T$$

The time-stepping iterative method is employed for the solution of the mean steady and unsteady perturbation equations. A shock-capturing scheme (NND) created by Zhang[1] is used in the space discretization. LU-SGS, created by Yoon and Jameson,[2] is used in an implicit iterative mode. The computational procedure is first to compute the mean flowfield, and then all of the coefficients for the first-order equations and the perturbed boundary conditions can be computed. Simultaneous solutions of the first-order equations are then obtained.

The numerical solutions are computed with a C-type grid having 128 × 65 grid nodes, the normal distance of the first point away from the body surface is nearly 10^{-3} radius lengths, the locations of the outer boundary are removed from the body by 10 radius lengths. The computed time step was taken as $\Delta t = 0.01$. For the zeroth equation, as a result of calculating the flowfield at zero incidence, a steady flow case takes 600 time stepping to reach the density residual error of 10^{-4}. For the first-order coupled equations, because of their linearity, the residual tends to be stable at only about 200 iterations, but the residual error dropped two orders of magnitude, this point may be caused by the numerical error of zeroth-order flowfield.

Results and Discussion

Zeroth-Order Calculated Result

The steady-state solution for the surface pressure for the four-caliber ogive-nose-cylinder was obtained directly from the zeroth-order equations shown by the solid curves in Fig. 1. The steady-state solution compares satisfactorily with experimental data[3] at zero incidence. Thus, the mean steady flow solution, which was used as the input for the unsteady flow calculation, is validated.

Quasisteady Perturbation Solution

In the previous equations, if the oscillation frequency $\omega = 0$, the perturbation equations at fixed incidence can be obtained. The steady flow can be divided into a mean steady and a real linearized perturbation equation. The quasisteady solution for the perturbed surface pressure is shown in Fig. 2. Because the perturbed flowfield is linear with respect to the incidence, the magnitude of $\Delta C_p/\alpha$ is plotted and compared with experimental data for $\alpha = \pm 4$ deg and $\alpha = \pm 8$ deg. Figure 2 shows that the agreement between theoretical and experimental results is excellent, indicating that linearity of the perturbed flow was realized up to an 8-deg incidence. Solving two two-dimensional coupled equations instead of solving the three-dimensional Euler equations up to 8-deg incidence will save large amounts of computer storage and time, implying the significance of this method in engineering applications.

Unsteady Perturbation Solution

Figure 3 gives the perturbation surface pressure for different reduced frequencies and Mach numbers. At the low reduced frequency $k = 0.01$, the imaginary part of perturbed pressure is approximately zero, indicating that the flow is nearly a quasisteady flow. For reduced frequency $k = 0.05$, the real part of the perturbed pressure is virtually unchanged with reduced frequency, but the changes of its imaginary part are obvious, and its changes appear to be a nonlinear character with reduced

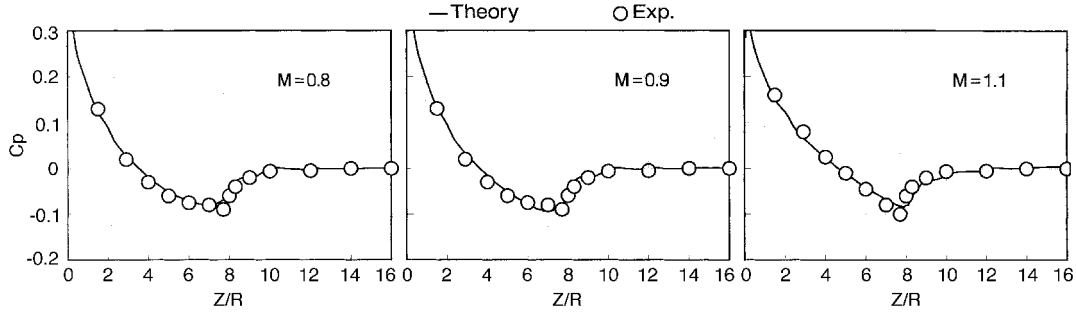

Fig. 1 Comparison with the experiment of steady surface pressure for a four-caliber ogive-nose-cylinder.

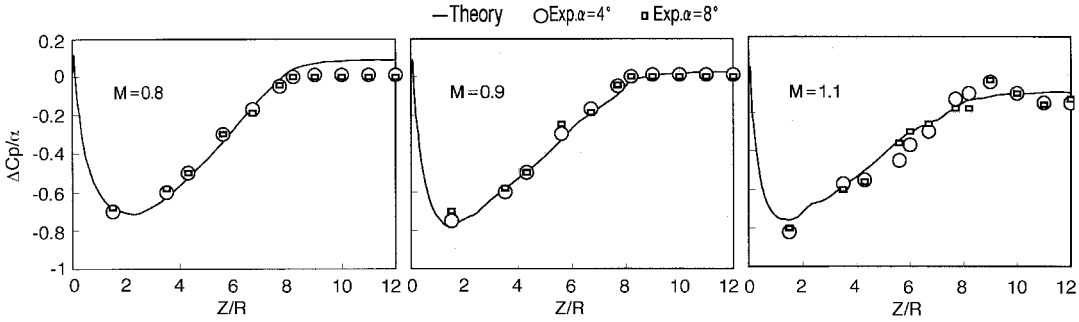

Fig. 2 Comparison with the experiment of quasisteady surface pressure for four-caliber ogive-nose-cylinder.

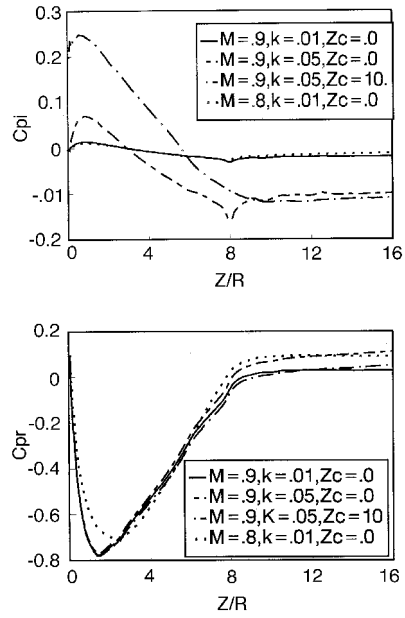

Fig. 3 Real and imaginary parts of unsteady surface pressure for a four-caliber ogive–nose–cylinder.

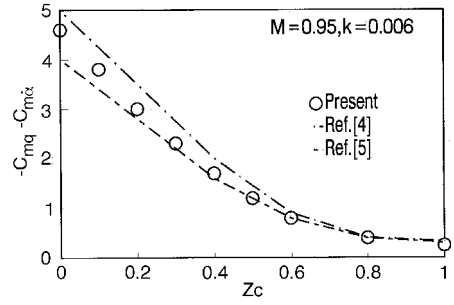

Fig. 4 Comparison of dynamic stability derivative vs pitching center for a parabolic arc nose.

frequency; it indicates a nonlinear dependence of the pitch-damping coefficient on reduced frequency. The conclusion is also suitable for the results with the variation of pitching center. For different Mach numbers (M = 0.8 and 0.9), the imaginary part is nearly unchanged, but the real part is changed, and the variations of the real part are similar to those of the quasisteady pressure.

No experimental data of dynamic stability derivatives are available for comparison. The dynamic derivative for a parabolic-arc nosed body are calculated by the present theory, and a comparison with results of the theory of Liu et al.[4] as well as Hsieh's[5] perturbation potential solution is made. The total damping-in-pitch coefficient versus pitching center is shown in Fig. 4. It indicates that the results of this theory have the same general tendency as Liu's and Hsieh's, but when the pitching center is close to the nose of the body, differences between the various theoretical appear. The result of the present theory lies between those of Liu's and Hsieh's theories. Therefore, the present theory seems equally capable of predicting dynamic stability derivatives.

Conclusions

A perturbation theory and numerical solution based on the unsteady Euler equations were developed for unsteady transonic flows about sharp-nosed bodies of revolution undergoing harmonic oscillations. The following conclusions can be drawn.

1) The quasisteady solution for the perturbation surface pressure for the sharp-nosed body of revolution agrees well with experimental results.

2) The unsteady results for a total damping-in-pitch coefficient agree well with results of the available calculation for a parabolic-arc nose. Although no experiment measurements for comparison are available, based on the analysis, the unsteady surface perturbation pressures are reasonable.

3) The theory is easily extended to treat three-dimensional unsteady flows on various configurations without limitation bodies of revolution. In engineering application, the theory may be efficient and effective for the prediction of unsteady flows and dynamic stability derivatives at small incidence.

Acknowledgments

The authors thank Zhuang Li-Xian, of the University of Science and Technology of China, for valuable discussions. The research was supported by the JSPS cooperation programs with southeast Asian countries under the core university system.

References

[1]Zhang, H., "Non-Oscillatory Containing No Free Parameter and Dissipative Scheme," *ACTA Aerodynamica Sinica*, Vol. 6, No. 2, 1989, pp. 145–155.

[2]Yoon, S., and Jameson, A., "An LU-SSOR Scheme for the Euler and Navier-Stokes equations," AIAA Paper 87-0600, Jan. 1987.

[3]Hartley, M. S., and Jacocks, J. L., "Static Pressure Distributions on Various Bodies of Revolution at Mach Numbers from 0.6 to 1.6," Arnold Engineering and Development Center, TR-68-37, March 1968.

[4]Liu, D. D., Platzer, M. F., and Ruo, S. Y., "Unsteady Linearized Transonic Flow Analysis for Slender Bodies," *AIAA Journal*, Vol. 15, No. 7, 1977, pp. 966–973.

[5]Hsieh, T., "Perturbation Solutions of Unsteady Transonic Flow over Bodies of Revolution," *AIAA Journal*, Vol. 16, No. 12, 1978, pp. 1271–1278.

Enhanced Multiobjective Technique for Multidisciplinary Design Optimization

John N. Rajadas,* Ralph A. Jury IV,†
and Aditi Chattopadhyay‡
Arizona State University, Mesa, Arizona 85206

Introduction

THE design of modern-day aircraft is a multidisciplinary process involving the integration of several disciplines such as aerodynamics, structures, dynamics, and propulsion, where optimization techniques that are able to address the different disciplines simultaneously are valuable tools. One such optimization technique is the Kreisselmeier–Steinhauser (K–S) function approach.[1] The K–S technique is a multiobjective optimization technique that combines all of the objective functions and the constraints to form a single unconstrained composite function that is then minimized using an appropriate unconstrained solver. The technique has been

Presented as Paper 97-0104 at the 35th Aerospace Sciences Meeting, Reno, NV, Jan. 6–9, 1997; received Sept. 8, 1997; revision received April 15, 1998; accepted for publication April 27, 1998.

*Department of Manufacturing and Aeronautical Engineering Technology. Senior Member AIAA.

†Department of Mechanical and Aerospace Engineering. Member AIAA.

‡Department of Mechanical and Aerospace Engineering. Associate Fellow AIAA.